Influence of the Sensitizer Adsorption Mode on the Open-Circuit Potential of Dye-Sensitized Solar Cells

Filippo De Angelis,*,† **Simona Fantacci,†** **Annabella Selloni,‡** **Michael Grätzel,§** and **Mohammed K. Nazeeruddin*,§**

Istituto CNR di Scienze e Tecnologie Molecolari (ISTM-CNR), c/o Dipartimento di Chimica, Università di Perugia, Via elce di Sotto 8, I-06213, Perugia, Italy, Department of Chemistry, Princeton University, Princeton, New Jersey, 08544, and Laboratory for Photonics and Interfaces, Station 6, Institute of Chemical Sciences and Engineering, School of basic Sciences, Swiss Federal Institute of Technology, CH-1015 Lausanne, Switzerland

ABSTRACT

We report a combined experimental and theoretical study on the origin of the different open circuit potentials observed in dye-sensitized solar cells using Ru(II)-polypyridyl homoleptic and heteroleptic sensitizers. We have measured the photovoltaic data of different sensitizers and used DFT calculations to analyze the electronic structure of dye-sensitized TiO$_2$ nanoparticles. Heteroleptic sensitizers adsorb onto TiO$_2$ via a single bipyridine, leading to a TiO$_2$ conduction band downshift and overall reduction of the cell open circuit potential.

Within today's global challenge to capture and utilize solar energy for a sustainable development on a grand scale, dye-sensitized solar cells (DSSCs) represent a particularly promising approach to the direct conversion of light into electrical energy at low cost and with high efficiency.[1−6] In these devices, a dye sensitizer absorbs the solar radiation and transfers the photoexcited electron to a wide band gap semiconductor electrode consisting of a mesoporous oxide layer composed of nanometer-sized particles, while the concomitant hole is transferred to the redox electrolyte.[7] Various ruthenium (II) complexes are employed primarily as dye sensitizers,[8] with carboxylic acid, dihydroxy, and phosphonic acid groups on the pyridine ligands anchoring the dyes on the surface of the oxide, typically TiO$_2$, nanoparticles. The remarkable performance of the tetraprotonated [cis-(dithiocyanato)-Ru-bis(2,2′-bipyridine-4,4′-dicarboxylate)] complex (N3) and its doubly protonated analogue (N719), see Figure 1, had a central role in significantly advancing the DSSC technology.[9] For further progress, however, higher conversion efficiencies need to be achieved. To this end, new sensitizers and a deeper understanding of the interaction between the dye and the TiO$_2$ nanoparticle are essential.

The overall conversion efficiency (η) of the DSSC is determined by the photocurrent density (i_{ph}), the open circuit potential (V_{oc}), the fill factor (ff) of the cell, and the intensity of the incident light (I_s), namely

$$\eta = i_{ph} \, V_{oc} \, ff/I_s$$

It was found that η markedly depends on several detailed features of the sensitizer, such as the number of protons carried by the sensitizer's anchoring groups.[10,11] Indeed, upon adsorption some of these protons may be transferred to the TiO$_2$ surface.[12] The resulting electric field assists electron injection, favoring higher photocurrents. However, the proton-induced positive shift of the Fermi level decreases the gap between the electrolyte redox couple and the TiO$_2$ conduction band, resulting in a lower open-circuit potential.

Molecular engineering together with advanced quantum chemical calculations have been employed in order to find new and more efficient sensitizers.[13−18] Starting from the N3 or N719 homoleptic sensitizers (**HMS**s), which have two equivalent bipyridine ligands, heteroleptic sensitizers (**HTS**s) have been devised in which one of the two bipyridines is specifically functionalized to obtain increased DSSCs' performances. In this context, the ruthenium (II) N621, K19, and N945 **HTS**s, see Figure 1, have been synthesized with the intent to increase the solar cell stability toward water-

* Corresponding author. E-mail: filippo@thch.unipg.it (FDA).
† ISTM-CNR.
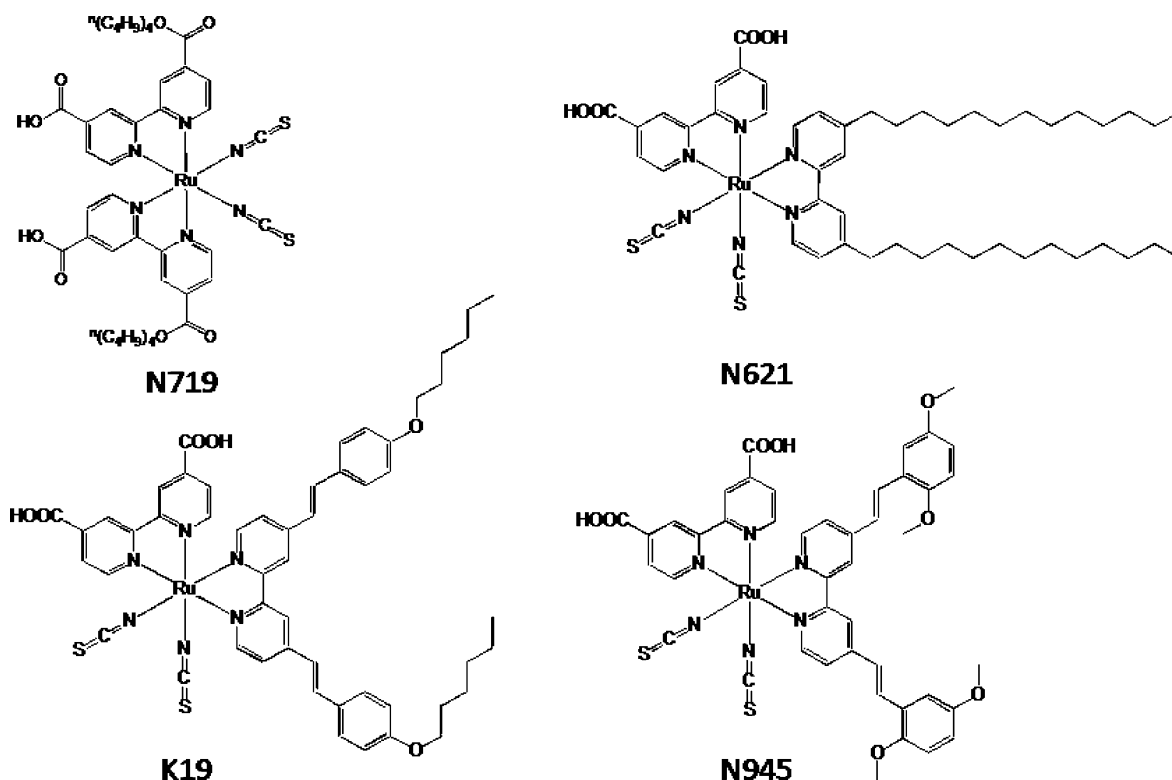‡ Princeton University.
§ Swiss Federal Institute of Technology.

Figure 1. Chemical structures of the N719, N621, K19, and N945 sensitizers.

induced desorption (N621),[13,19] and the sensitizer molar extinction coefficient (K19 and N945),[18,20] thereby enhancing its light-harvesting capability. Quite unexpectedly, however, experiments have shown that the V_{oc} for DSSCs employing **HTS**s is significantly lower compared to that observed using **HMS**s containing the same number of protons.[13,18−20] Because the chemical functionalization of one bipyridine has little effect on the electronic properties of the second bipyridine,[13] the difference between **HMS**s and **HTS**s is likely to originate from the different adsorption modes of the two types of complexes onto the TiO₂ surface. Indeed, although **HMS**s such as N719 can adsorb on TiO₂ using carboxylic anchoring groups residing on different bipyridines, **HTS**s necessarily adsorb via carboxylic groups residing on the same bipyridine.

Several investigations have addressed the sensitizer interaction with nanocrystalline TiO₂ films[21] and the dynamics of the electron injection.[22,23] However, the influence of the sensitizer adsorption mode on the DSSC photovoltage has not yet been examined. Clarification of this question is vital for the design of efficient sensitizers and thereby for the improvement of DSSCs. In this work, we report on a combined experimental and theoretical study aimed at understanding the origin of the different open circuit potentials observed in solar cells using **HMS**s and **HTS**s. On the experimental side, we have measured the photovoltaic data of **HMS**s and **HTS**s (N719, N621, K19, and N945) under similar conditions. This data has been theoretically analyzed by means of state-of-the-art density functional theory (DFT) calculations on representative **HMS**s and **HTS**s adsorbed on a TiO₂ nanoparticle model in different configurations. We find that the adsorption geometry of **HTS**s

Table 1. Photovoltaic Parameters of Dye-sensitized Solar Cells with N719, N621, K19, and N945 Sensitizers

sensitizer	number of protons	current (mA/cm²⁾	potential (mV)	fill factor	efficiency at 1.5 AM
N719	2	16.66	846	0.73	10.28
N621	1	16.22	766	0.70	8.69
K19	1	16.40	768	0.73	9.19
N945	1	17.25	759	0.73	9.55

induces a substantial downshift of the TiO₂ conduction band energy, ultimately causing reduced photovoltages, possibly because of the different dipolar fields exerted on the TiO₂ surface by **HMS**s and **HTS**s. A dipole-induced conduction band shift is effectively confirmed by calculations in which artificial dipolar fields are applied to the TiO₂ nanoparticle.

We report in Table 1 the photovoltaic data of **HMS**s and **HTS**s, measured under AM 1.5 conditions (see the Methods Section for details). We notice that similar *ff* and i_{ph} values are measured for all sensitizers, except for N945, which shows slightly higher photocurrent density because of its enhanced molar extinction coefficient. Alternatively, the observed V_{oc} for N719 is ∼80 mV higher than the corresponding quantity measured for the investigated **HTS**s. The increased open-circuit potential of N719 represents only a lower bound because N719 carries two protons while the investigated **HTS**s carry only one proton so that an even larger photovoltage difference of ca.150−170 mV may be expected for sensitizers with the same number of protons. For N719, a reduction of the number of protons from 2 to 1 was indeed found to induce a photovoltage increase as large as 90 mV.[24]

To understand the origin of such experimental observations, we have performed DFT calculations (see the Methods
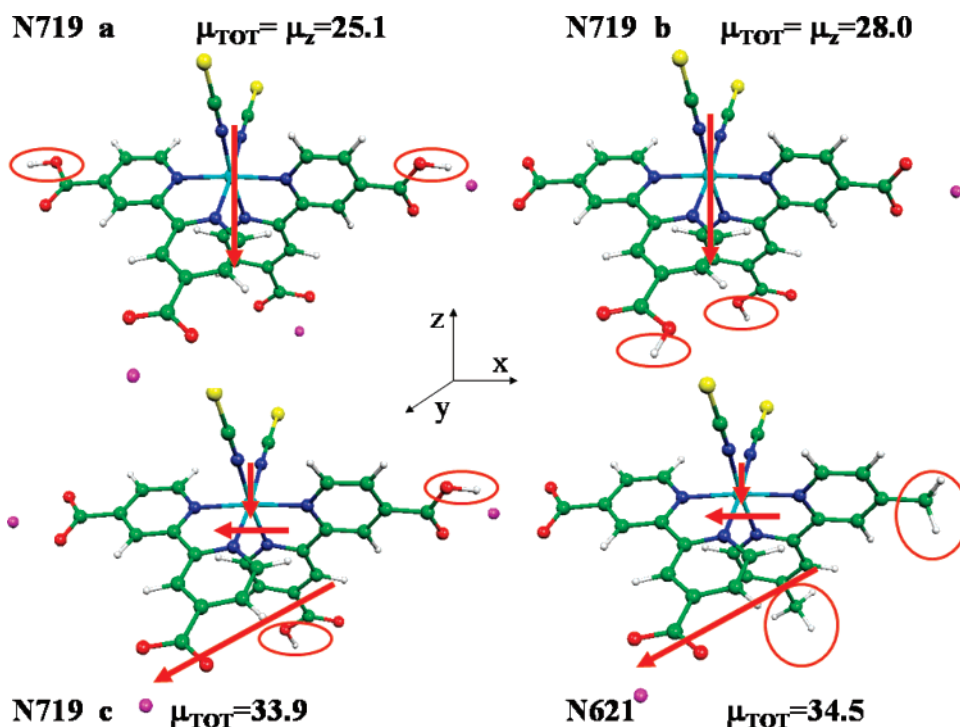
Figure 2. Optimized geometrical structures of **a**, **b**, and **c** N719 sensitizers and of the N621 model, along with dipole moments magnitudes and directions.

Section for details) to analyze the electronic structure of representative dyes, specifically the different N719 isomers and N621 (see Figure 2), adsorbed on a TiO_2 anatase nanoparticle. We start by considering the isolated doubly protonated N719 and deprotonated N621 complexes in water, including in both cases two Na^+ counterions.[13] As shown in Figure 2, three different isomers of N719 can be identified: **a** and **b** for which the two protons are located on the carboxylic groups cis and trans, respectively, to the NCS ligands; and **c**, where the protonated carboxyls are one in cis and the other in trans positions, resulting in two nonequivalent bipyridine ligands. Although very similar (within ∼1.5 kcal/mol), the computed total energies indicate that **a** and **b** are more stable than **c**. This is consistent with NMR data for N719, which appear to rule out the occurrence of the **c** isomer.[13] In the following, however, all three isomers will be considered: the **a** and **b** isomers represent typical **HMS**s, whereas **c** and N621 are representative of **HTS**s. The three N719 isomers have different charge distributions, as revealed by the different moduli and directions of the calculated dipole moments (throughout this paper, we assume that the dipole moment points from negative to positive charge). The dipole moments, μ, of the **a** and **b** isomers are comparable in sign and magnitude, and both are directed along the z axis (Figure 2): in both isomers, the contributions from the negatively charged thiocyanate ligands dominate, leading to $\mu = -27.8$ and -28.0 D in **a** and **b**, respectively, see Figure 2 and Table 2. In **c**, the charge asymmetry deriving from having protonated the carboxylic groups trans and cis to the NCS ligands results in large transversal dipole components, particularly along the y axis (30.6 D), whereas the z component is reduced considerably (-9.8 D). Overall, the magnitude of μ is larger for **c** (33.9 D) than for **a** and **b**.

Table 2. Calculated Dipole Moments for the **a**−**c** N719 Isomers and for the N621 Sensitizer in the Geometry and Orientation Corresponding to the Free (Figure 2) and Adsorbed (Figure 3) Dye

	free dye			adsorbed dye		
sensitizer	dipole components			dipole components		
	μ_x	μ_y	μ_z	μ_x	μ_y	μ_z
N719 **a**	0.0	0.0	−25.0	−8.6	4.7	−23.1
N719 **b**	0.0	0.0	−28.0			
N719 **c**	−10.7	30.6	−9.8	−17.2	3.4	−29.0
N621	−7.0	32.7	−8.6	−16.8	1.8	−30.1

For the N621 sensitizer, we compute a μ magnitude of 34.5 D, only slightly larger than that of **c**, see Table 2 for a summary of calculated dipole moments.

To investigate how the sensitizer's adsorption mode influences the electronic structure of the combined sensitizer/TiO_2 nanoparticle system, we examined four prototypical configurations, formally resulting from the adsorption of the **a**−**c** N719 isomers onto the TiO_2 nanoparticle model. The optimized structures of these four configurations are shown in Figure 3: **A** (**B**) corresponds to adsorption through deprotonated (protonated) carboxylic groups belonging to *different* bipyridines, whereas **C′** (**C″**) corresponds to adsorption through deprotonated (protonated) carboxylic groups belonging to the *same* bipyridine. In addition to the above structures, a configuration originated from **C′** was also studied, in which the protonated carboxylic groups were replaced by alkyl groups, to effectively represent the heteroleptic deprotonated N621 complex; this will be denoted **C′**-N621. Notice that the same z-axis orientation is used in Figures 2 and 3, that is, for the free and adsorbed dye,
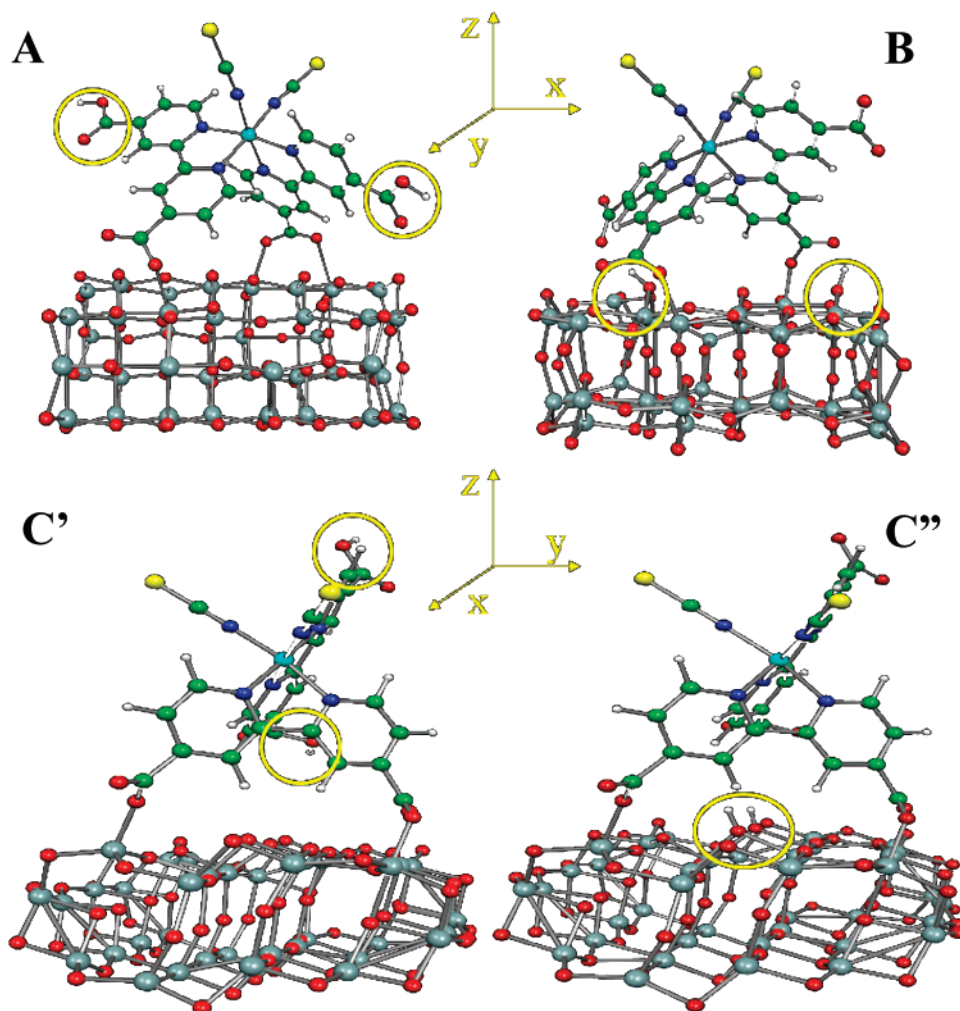
Figure 3. Optimized geometrical structures of the four considered N719 adsorption modes. The circles indicate the position of the two protons. Notice that, for a better structure visualization, the *x* and *y* axis are exchanged in **C′/C″** compared to **A/B** configurations.

whereas the *x* and *y* axis are exchanged for **C′/C″** in Figure 3. We find that in the **B** and **C″** configurations the two protons of the sensitizer are transferred to coordinatively unsaturated twofold oxygens of the TiO$_2$ surface upon adsorption, whereas in **A** and **C′** they are retained on the dye (**C′**-N621 carries no protons). Although additional N719 adsorption geometries on TiO$_2$ might exist, those considered here allow us to separately investigate the roles of TiO$_2$ protonation and sensitizer adsorption geometry, as well as to perform a direct comparison between homoleptic (**A** and **B**) and heteroleptic (**C′**, **C″** and **C′**-N621) sensitizers under similar conditions. In fact, in all cases the sensitizer adsorbs via two carboxylic groups, and the essential difference between **A** and **C′** and between **B** and **C″** is the adsorption geometry.

In Figure 4, orbital energy diagrams for the four N719 adsorption configurations are reported. For the isolated N719 and N621 sensitizers in solution, the highest occupied molecular orbitals (HOMOs) are antibonding combinations of Ru(t$_{2g}$) and NCS (π*) orbitals.[13−16,18,25] In the three N719 isomers, these have almost identical energies and character. The lowest unoccupied molecular orbitals (LUMOs) of the isolated sensitizers are π* combinations localized on the pyridines bearing the protonated carboxylic groups, with the

corresponding orbitals localized on the deprotonated pyridines lying at slightly higher energies.[13,15] Upon adsorption onto the TiO$_2$ nanoparticle, the molecular HOMOs insert within the TiO$_2$ band gap so that the HOMO of the combined sensitizer/TiO$_2$ system basically corresponds to that of the isolated sensitizer (Figure 4), whereas the top of the TiO$_2$ valence band lies at lower energy. By contrast, for all of the investigated dye/TiO$_2$ systems the LUMO has the character of a TiO$_2$ conduction band state (Figure 4), with the sensitizer's unoccupied orbitals almost overlapping the bottom of the TiO$_2$ conduction band. In addition, remarkable differences are found in the energies and character of the LUMOs depending on the position of the two protons and the sensitizer's adsorption geometry. Adsorption of the two protons onto the TiO$_2$ surface in the **B** and **C″** configurations leads to a downshift of the TiO$_2$ conduction band edge compared to **A** and **C′** by 0.08 and 0.51 eV, respectively. This proton-induced downshift, considerably more pronounced for **C′/C″**, is in agreement with the experimentally characterized reduced V_{OC} measured for sensitizers containing protons,[24] as mentioned above. Associated with the energy downshift, a considerable mixing of the sensitizer π* orbitals with TiO$_2$ conduction states takes place: although in **A** the LUMO+1 is essentially a pure N719 π* orbital, for **B** a
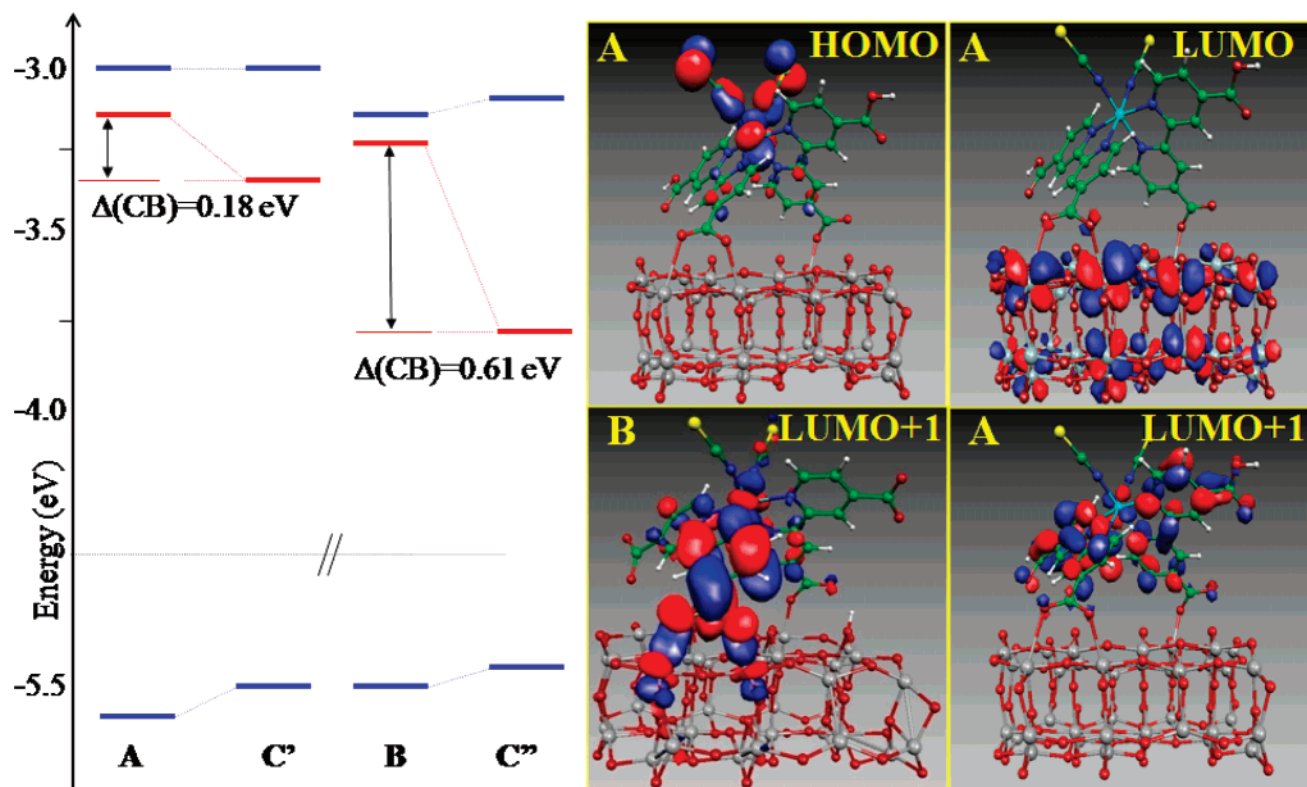
Figure 4. Schematic representation of the HOMOs and LUMOs of the **A**, **B**, **C′**, and **C″** configurations of N719 adsorbed onto TiO$_2$. Energy in eV. Blue (red) lines refer to lowest energy levels maximally localized on the sensitizer (TiO$_2$). Isodensity plots of representative molecular orbitals are also reported.

mixed state is found (Figure 4). The mixing of sensitizer π^* orbitals and TiO$_2$ conduction band states increases the electronic coupling between the sensitizer and the semiconductor,[26] eventually leading to increased photocurrents. A similar picture of the occupied and unoccupied molecular orbitals holds for **C′** and **C″**.

An important result of our calculations is that, besides protonation, the sensitizer's adsorption mode also affects the position of the TiO$_2$ conduction band edge. Indeed, by comparing the energy levels of **A** and **C′**, and of **B** and **C″** (Figure 4), it appears that for a given number of protons (0 or 2) transferred to the surface the systems where the sensitizer is adsorbed via a single bipyridine ligand have the TiO$_2$ conduction band edge at significantly lower energies with respect to the systems in which the sensitizer is adsorbed through two different bipyridines. This effect is not limited to the edge but to the entire conduction band. Specifically, a 0.18 eV downshift is found for **C′** with respect to **A**, and an even larger shift, 0.61 eV, occurs for **C″** with respect to **B**. The TiO$_2$ conduction band edge downshift in the **C′** and **C″** geometries is so pronounced that the lowest π^* states of the sensitizer correspond to the LUMO+6/LUMO+8 of the combined sensitizer/nanoparticle system. The position of the TiO$_2$ conduction band edge for **C′**-N621 is essentially the same as that for **C′**, confirming that the effect is related to the adsorption geometry rather than to the details of the sensitizer's electronic structure. These results agree well with the photovoltaic data in Table 1, supporting the idea that

the sensitizer adsorption mode is the origin of the reduced V_{oc} values experimentally observed for the N621, N945, and K19 **HTS**s.

The differences in the computed orbital energy diagrams of Figure 4 may be surprising. Because the essential difference between the three N719 isomers is in their charge distributions, these results suggest that the sensitizer dipole moment can influence the position of the TiO$_2$ conduction band. An analogous effect has been observed using coadsorbed dipolar molecules to modify the electronic properties of the TiO$_2$ electrode.[27] Notably, it was found that coadsorbed molecules with a dipole pointing toward the surface plane cause a decrease of the open circuit potential, whereas the opposite is true for a dipole pointing opposite to the surface.[27] A related and extensively studied effect is also the modification of metal surface workfunctions with adsorbed monolayers of dipolar molecules, such in the case of alkanethiols on gold surfaces.[28,29]

The sensitizer dipoles for the N719 **a** and **c** isomers and for N621 obtained using the geometrical arrangement relative to the TiO$_2$ surface calculated for the **A**, **C′**, and **C′**-N621 configurations are reported in Table 2. We notice that the configurations leading to decreased values of the TiO$_2$ conduction band edge (**C′** and **C′**-N621) show an increased dipole moment component normal to the TiO$_2$ surface plane (the z component), with the dipole pointing toward the surface. As a demonstration of the influence of dipolar fields on the position of the TiO$_2$ conduction band, we computed the electronic structure of the bare TiO$_2$ nanoparticle in
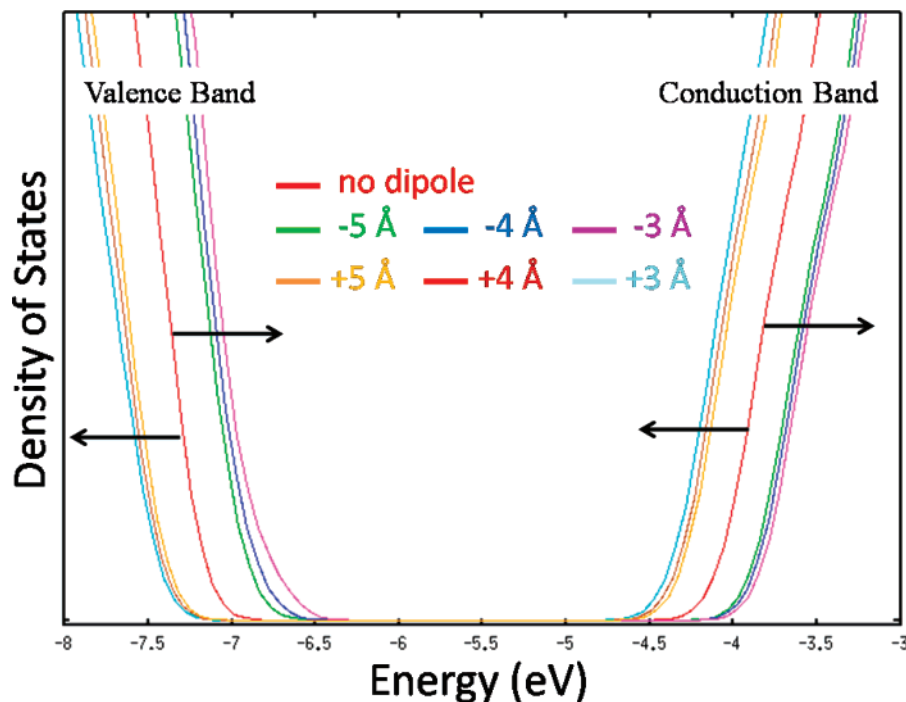
Figure 5. Densities of states for the bare TiO$_2$ nanoparticle subject to different dipolar fields along the $\pm z$ directions. The red curve corresponds to the density of states in absence of the field. The magenta, blue, and green lines correspond to a 30 D dipole pointing away from the surface lying 3, 4, and 5 Å, respectively, above the surface. The light-blue, brown, and orange lines correspond to a 30 D dipole pointing toward the surface lying 3, 4, and 5 Å, respectively, above the surface.

presence of a dipole applied in the direction normal to the surface plane ($\pm z$). The resulting densities of states are shown in Figure 5. When the applied dipole points toward the surface, a downshift of a few tenths of an electronvolt of both the valence and conduction band of the TiO$_2$ nanoparticle is observed. Vice versa, for a dipole pointing away from the surface, a similar upshift of the bands takes place. On the basis of these results, which agree very well with the experiment,[27] it seems that the TiO$_2$ conduction edge downshifts of **C′** versus **A** and **C″** versus **B** can be related to the different orientation of the sensitizers' dipole moments associated to different adsorption geometry found for the **C′/C″** compared to the **A/B** configurations.

In conclusion, on the basis of a combined experimental and first-principles theoretical study, we have shown that the sensitizer adsorption geometry on the TiO$_2$ surface has a remarkable influence on the open circuit potential and ultimately on the efficiency of dye-sensitized solar cells. In particular, heteroleptic sensitizers with anchoring sites localized on the same bipyridine ligand, such as N621, N945, and K19, give rise to a decrease of the open circuit potential because of the different sensitizer adsorption mode onto TiO$_2$ compared to homoleptic sensitizers. Associated with the different adsorption mode, dipolar fields of different magnitude and orientation are found for homoleptic sensitizers with anchoring groups residing on two different bipyridines, like N3 or N719, which explains their larger open circuit potentials and overall better performances with respect to heteroleptic sensitizers. Our results provide the necessary framework for the design of new and more-efficient solar cell sensitizers and devices.

Method. We report in Table 1 the photovoltaic data of homoleptic and heteroleptic sensitizers (see Figure 1 for structures) measured under AM 1.5 conditions using TiO$_2$ films having $12 + 4$ μm thickness and with an electrolyte consisting of 0.60 M 1-butyl-3-methylimidazolium iodide (BMII), 0.03 M I$_2$, 0.10 M guanidinium thiocyanate, and 0.50 M *tert*-butylpyridine in a mixture of acetonitrile and valeronitrile (volume ratio 85:15). The first layer (of thickness 12 μm) was prepared using 20 nm TiO$_2$ particles, and for the second layer (4 μm thick) 400-nm TiO$_2$ particles were used.[30] After treating the TiO$_2$ films with 40 mM TiCl$_4$, they were rinsed with water, followed by ethanol, and sintered at 500 °C for 30 min. Then the TiO$_2$ electrodes were allowed to cool to 80 °C, immersed into dye solutions (0.5 mM in a mixture of acetonitrile and *tert*-butyl alcohol (volume ratio 1:1)), and kept at room temperature for 20−24 h.

To model the TiO$_2$ nanoparticle, we used a (TiO$_2$)$_{38}$ cluster,[31−33] obtained by appropriately "cutting" an anatase slab exposing the majority (101) surface.[34] All atomic structures were optimized by means of Car−Parrinello (CP) molecular dynamics[35] using the PBE exchange-correlation functional[36] together with a plane wave basis set and ultrasoft pseudopotentials.[37] The considered cluster represents a good tradeoff between accuracy and computational convenience and nicely reproduces the main electronic characteristics of TiO$_2$ nanoparticles. Indeed, the lowest transition of the (TiO$_2$)$_{38}$ cluster calculated using time-dependent DFT is 3.20 eV,[30] in good agreement with the experimental bandgaps typical of TiO$_2$ nanoparticles of a few nanometers size (3.2−3.3 eV).[38] The CP calculations were followed by single-point electronic structure analysis in solution, for which we used

the hybrid B3LYP functional[39] together with a DZVP basis set,[40] in conjunction with a polarizable continuum model of solvation (C-PCM),[41] as implemented in the Gaussian03 program package.[42] For the dyes adsorbed on the TiO_2 nanoparticle, we did not consider any counterion. For the N621 sensitizer, we use a reduced model in which the alkyl chains are replaced by methyl groups; this model was shown to represent the electronic properties of the real complex accurately.[13]

References

(1) O'Regan, B.; Grätzel, M. *Nature* **1991**, *353*, 737.
(2) Rehm, J. M.; McLendon, G. L.; Nagasawa, Y.; Yoshihara, K.; Moser, J.; Grätzel, M. *J. Phys Chem B* **1996**, *100*, 9577.
(3) Hagfeldt, A.; Grätzel, M. *Chem. Rev.* **1995**, *95*, 49.
(4) Grätzel, M. *Nature* **2001**, *414*, 338−344.
(5) Nazeeruddin, M. K.; Wang, Q.; Cevey, L.; Aranyos, V.; Liska, P.; Figgemeier, E.; Klein, C.; Hirata, N.; Koops, S.; Haque, S. A.; Durrant, J. R.; Hagfeldt, A.; Lever, A. B. P.; Grätzel, M. *Inorg. Chem.* **2006**, *45*, 787.
(6) Kamat, P. V. *J. Phys. Chem C* **2007**, *111*, 2834.
(7) Nazeeruddin, M. K.; Grätzel, M. in *Molecular and Supramolecular Photochemistry*; Ramamurthy, V., Schanze, K. S.; Marcel Dekker: New York, 2003; p 301; Vol. 10.
(8) Grätzel, M. *C. R. Chim.* **2006**, *9*, 578.
(9) Nazeeruddin, M. K.; Kay, A.; Rodicio, I.; Humphry-Baker, R.; Muller, E.; Liska, P.; Vlachopoulos, N.; Grätzel, M. *J. Am. Chem. Soc.* **1993**, *115*, 6382.
(10) Yan, S. G.; Hupp, J. T. *J. Phys. Chem.* **1996**, *100*, 6867.
(11) Tachibana, Y.; Haque, S. A.; Mercer, I. P.; Moser, J. E.; Klug, D. R.; Durrant, J. R. *J. Phys. Chem. B* **2001**, *105*, 7424.
(12) Nazeeruddin, M. K.; Zakeeruddin, S. M.; Humphry-Baker, R.; Jirousek, M.; Liska, P.; Vlachopoulos, N.; Shklover, V.; Fischer, C. H.; Grätzel, M. *Inorg. Chem.* **1999**, *38*, 6298.
(13) Nazeeruddin, M. K.; De Angelis, F.; Fantacci, S.; Selloni, A.; Viscardi, G.; Liska, P.; Ito, S.; Takeru, B.; Grätzel, M. *J. Am. Chem. Soc.* **2005**, *127*, 16835.
(14) Fantacci, S.; De Angelis, F.; Selloni, A. *J. Am. Chem. Soc.* **2003**, *125*, 4381.
(15) De Angelis, F.; Fantacci, S.; Selloni, A. *Chem. Phys. Lett.* **2004**, *389*, 204.
(16) De Angelis, F.; Fantacci, S.; Selloni, A.; Nazeeruddin, M. K. *Chem. Phys. Lett.* **2005**, *415*, 115.
(17) Barolo, C.; Nazeeruddin, M. K.; Fantacci, S.; Di Censo, D.; Comte, P.; Liska, P.; Viscardi, G.; Quagliotto, P.; De Angelis, F.; Ito, S.; Grätzel, M. *Inorg. Chem.* **2006**, *45*, 4642.
(18) Nazeeruddin, M. K.; Bessho, T.; Cevey, L.; Ito, S.; Klein, C.; De Angelis, F.; Fantacci, S.; Comte, P.; Liska, P.; Imai, H.; Grätzel, M. *J. Photochem. Photobiol., A* **2007**, *185*, 331.
(19) Nazeeruddin, M. K.; Zakeeruddin, S. K.; Lagref, J.-J.; Barolo, C.; Viscardi, G.; Liska, P.; Comte, P.; Schenk, K.; Grätzel, M. *Coord. Chem. Rev.* **2004**, *248*, 1317.
(20) Wang, P.; Klein, C.; Humphry-Baker, R.; Zakeeruddin, S. M.; Grätzel, M. *J. Am. Chem. Soc.* **2004**, *126*, 808.
(21) Finnie, K. S.; Bartlett, J. R.; Woolfrey, J. L. *Langmuir* **1998**, *14*, 2744.
(22) Tachibana, Y.; Nazeeruddin, M. K.; Grätzel, M.; Klug, D. R.; Durrant, J. R. *Chem. Phys.* **2002**, *284*, 127.
(23) Moser, J. E.; Noukakis, D.; Bach, U.; Tacchibana, Y.; Klug, D. R.; Durrant, J. R.; Humphry-Baker, R.; Grätzel, M. *J. Phys. Chem. B* **1998**, *102*, 3649.
(24) Nazeeruddin, M. K.; Humphry-Baker, R.; Liska, P.; Grätzel, M. *J. Phys. Chem. B* **2003**, *107*, 8981.
(25) Rensmo, H.; Södergren, S.; Patthey, L.; Westmark, K.; Vayssieres, L.; Khole, O.; Brühwiler, P. A.; Hagfeldt, A.; Siegbhan, H. *Chem. Phys. Lett.* **1997**, *274*, 51.
(26) (a) Persson, P.; Lundqvist, M. J. *J. Phys. Chem. B* **2005**, *109*, 1191. (b) Duncan, W. R.; Craig, C. F.; Prezhdo, O. V. *J. Am. Chem. Soc.* **2007**, *129*, 8528.
(27) Rühle, S.; Greenshtein, M.; Chen, S.-G.; Merson, A.; Pizem, H.; Sukenik, C. S.; Cahen, D.; Zaban, A. *J. Phys. Chem. B* **2005**, *109*, 18907.
(28) Alloway, D. M.; Hofmann, M.; Smith, D. L.; Gruhn, N. E.; Graham, A. L.; Colorado, R.; Wysocki, V. H.; Lee, T. R.; Lee, P. A.; Armstrong, N. R. *J. Phys. Chem. B* **2003**, *107*, 11690.
(29) Sun, Q.; Selloni, A. *J. Phys Chem A* **2006**, *110*, 11396.
(30) Ito, S.; Nazeeruddin, M. K.; Liska, P.; Comte, P.; Charvet, R.; Pechy, P.; Jirousek, M.; Zakeeruddin, S. M.; Grätzel, M. *Prog. Photovoltaics* **2006**, *14*, 589.
(31) Persson, P.; Bergstrom, R.; Lunell, S. *J. Phys. Chem. B* **2000**, *104*, 10348.
(32) De Angelis, F.; Tilocca, A.; Selloni, A. *J. Am. Chem. Soc.* **2004**, *126*, 15024.
(33) Lundqvist, M. J.; Nilsing, M.; Lunell, S.; Akemark, B.; Persson, P. *J. Phys. Chem. B* **2006**, *110*, 20513.
(34) Vittadini, A.; Selloni, A.; Rotzinger, F. P.; Grätzel, M. *Phys. Rev. Lett.* **1998**, *81*, 2954.
(35) Car, R.; Parrinello, M. *Phys. Rev. Lett.* **1985**, *55*, 2471.
(36) Perdew, J. P.; Burke, K.; Ernzerhof, M. *Phys. Rev. Lett.* **1996**, *77*, 3865.
(37) a) Pasquarello, A.; Laasonen, K.; Car, R.; Lee, C.; Vanderbilt, D. *Phys. Rev. Lett.* **1992**, *69*, 1982−1985. b) Giannozzi, P.; De Angelis, F.; Car, R. *J. Chem. Phys.* **2004**, *120*, 5903.
(38) (a) Weng, Y. X.; Wang, Y. Q.; Asbury, J. B.; Ghosh, H. N.; Lian, T. *J. Phys. Chem B* **2000**, *104*, 93. (b) Khoudiakov, M.; Parise, A. R.; Brunschwig, B. S. *J. Am. Chem. Soc.* **2003**, *125*, 4637.
(39) Becke, A. D. *J. Chem. Phys.* **1993**, *98*, 5648.
(40) Godbout, N.; Salahub, D. R.; Andzelm, J.; Wimmer, E. *Can. J. Chem.* **1980**, *102*, 939.
(41) (a) Cossi, M.; Barone, V. *J. Chem. Phys.* **2001**, *115*, 4708. (b) Cossi, M.; Rega, N.; Scalmani, G.; Barone, V. *J. Comput. Chem.* **2003**, *24*, 669.
(42) Frisch, M. J.; Trucks, G. W.; Schlegel, H. B.; Scuseria, G. E.; Robb, M. A.; Cheeseman, J. R.; Montgomery, J. A., Jr.; Vreven, T.; Kudin, K. N.; Burant, J. C.; Millam, J. M.; Iyengar, S. S.; Tomasi, J.; Barone, V.; Mennucci, B.; Cossi, M.; Scalmani, G.; Rega, N.; Petersson, G. A.; Nakatsuji, H.; Hada, M.; Ehara, M.; Toyota, K.; Fukuda, R.; Hasegawa, J.; Ishida, M.; Nakajima, T.; Honda, Y.; Kitao, O.; Nakai, H.; Klene, M.; Li, X.; Knox, J. E.; Hratchian, H. P.; Cross, J. B.; Bakken, V.; Adamo, C.; Jaramillo, J.; Gomperts, R.; Stratmann, R. E.; Yazyev, O.; Austin, A. J.; Cammi, R.; Pomelli, C.; Ochterski, J. W.; Ayala, P. Y.; Morokuma, K.; Voth, G. A.; Salvador, P.; Dannenberg, J. J.; Zakrzewski, V. G.; Dapprich, S.; Daniels, A. D.; Strain, M. C.; Farkas, O.; Malick, D. K.; Rabuck, A. D.; Raghavachari, K.; Foresman, J. B.; Ortiz, J. V.; Cui, Q.; Baboul, A. G.; Clifford, S.; Cioslowski, J.; Stefanov, B. B.; Liu, G.; Liashenko, A.; Piskorz, P.; Komaromi, I.; Martin, R. L.; Fox, D. J.; Keith, T.; Al-Laham, M. A.; Peng, C. Y.; Nanayakkara, A.; Challacombe, M.; Gill, P. M. W.; Johnson, B.; Chen, W.; Wong, M. W.; Gonzalez, C.; Pople, J. A. *Gaussian 03*, revision C.02; Gaussian, Inc.: Wallingford, CT, 2004.

NL071835B